Journal of Materials Chemistry A

ROYAL SOCIETY OF CHEMISTRY

PAPER

View Article Online
View Journal | View Issue

Cite this: J. Mater. Chem. A, 2025, 13, 5723

Enhancing the durability of aluminium-foil anodes in rechargeable lithium batteries *via* uniformly distributed alloy addition in the matrix phase†

Hongyi Li, *[a] Shohei Nishimura,[a] Weiqi Liu,[a] Norihiko L. Okamoto, [a] Shingo Matsumoto,[b] Yuki Nakata,[b] Hiroaki Hoshikawa,[c] Toshiaki Kumagai,[c] Takitaro Yamaguchi[b] and Tetsu Ichitsubo *[a]

Al-foil anodes suffer from self-reinforcing pulverization and surface passivation in liquid electrolytes, which significantly limit their cyclability. From the perspective of structural materials, alloy additions to the Al matrix present a promising strategy for managing morphological changes to enhance the performance of Al-foil anodes. However, establishing design guidelines requires a clear understanding of the underlying mechanisms. In this study, we focus on Si, a typical alloy addition known for strengthening Al alloys, and prepare Al-*x*Si foils (x = 0–4 wt%) to investigate how Si distribution influences reaction behavior and electrode properties. At low concentrations (x < 1%), Si is uniformly distributed in the Al matrix as a solid solution. At higher concentrations (1% < x < 4%), Si tends to agglomerate into large, micrometer-sized Si particles. During electrode reactions, uniformly distributed Si in the Al matrix is prone to forming amorphous Li–Si(-Al) domains during lithiation, preventing cracks in the recrystallized Al phase during subsequent delithiation. In contrast, agglomerated Si particles have negligible effects on the reaction behavior of Al-*x*Si foil anodes. With the highest amount of uniformly distributed Si, Al-1%Si shows a stable interface with a limited surface area increase, resulting in superior cyclability in full cells with $LiCoO_2$ cathodes. On the other hand, the limited interface restricts the kinetics of Li extraction, causing irreversible capacity loss, which needs further improvement to facilitate bulk diffusion in the matrix.

Received 8th November 2024
Accepted 20th January 2025

DOI: 10.1039/d4ta07956f

rsc.li/materials-a

Introduction

Al foils have been expected to be used as anodes of rechargeable lithium batteries.[1] Basically, the alloy reaction of $Li^- + e^- + Al =$ LiAl can achieve a theoretical capacity of 993 mA h g^{-1}, which is much higher than that of graphite anodes (372 mA h g^{-1}) used in conventional Li-ion batteries. In addition, Al-foil anodes can eliminate inactive components, such as current collectors, conductive additives and polymer binders, simplifying the manufacturing process and reducing production costs. One of the main problems that has hindered the use of Al-foil anodes is their structural degradation due to the large volume change (+100%) associated with Li alloying, which is a general problem of alloy-based anode materials.[2,3] The LiAl alloy phase and the Al matrix have different crystal structures, resulting in distinctly different mechanical and chemical properties. This usually leads to plastic deformation or material failure during alloying, where the deformed LiAl phase or/and Al matrix would contain strain effects that disrupt the homogeneous reaction and accelerate structural degradation.[4]

To circumvent the strain effects during lithiation, the hardness of the Al matrix can be used as a control factor for the lithiation behavior.[5] By keeping LiAl and Al in the elastic deformation region, the strain effects can be uniformly distributed over the foil surface. Since the in-plane growth (isotropic volume expansion) of LiAl grains is limited by the surrounding Al matrix, a flat LiAl layer is uniformly formed on the foil surface during lithiation. In addition, the solubility range of the LiAl phase allows a concentration gradient to form in the out-of-plane direction. The concentration gradient drives the interdiffusion of Li and Al, and consequently the +100% volume expansion from Al to LiAl is confined in the out-of-plane direction. During delithiation, the Al phase is recrystallized from the LiAl layer associated with volume contraction and is typically self-organized into porous structures. The porous structure is usually preferred for electrode materials because the high surface area can improve reaction kinetics and the pores in the active materials can tolerate the reversible volume changes during cycling.[6] Based on this reaction behavior, Al-foil

[a]Institute for Materials Research, Tohoku University, Sendai 980-8577, Japan. E-mail: li.hongyi@tohoku.ac.jp; tichi@tohoku.ac.jp
[b]Advanced Materials Development Laboratory, Sumitomo Chemical Co., Ltd, Tsukuba 300-3294, Japan
[c]ICT & Mobility Solutions Research Laboratory, Sumitomo Chemical Co., Ltd, Ehime 792-8521, Japan

† Electronic supplementary information (ESI) available. See DOI: https://doi.org/10.1039/d4ta07956f

anodes can be divided into two functional layers. The surface layer serves as the active material, storing and releasing Li during cycling. On the other hand, the remaining unreacted base layer functions as a current collector that maintains structural stability and electrical conductivity. Thus, the areal capacity would be related to the ideal thickness of the surface layer, and the ratio of the surface layer in the Al foil would determine the total capacity density of Al-foil anodes.

Toward their applications, the following challenges limit the cyclability of Al-foil anodes in liquid electrolytes:[7–10] (i) porosification and thickening of the surface layer. The recrystallized Al particles in the surface layer become finer and finer in self-organization during repeated delithiation. The fine particles are readily detached from each other and lose electrical connection, resulting in structural degradation and capacity loss. (ii) Electrolyte decomposition products passivate the fine particles. The electrolyte is progressively decomposed on the fresh Al surface to form the solid-electrolyte interphase (SEI) as the porosification progresses during cycling causing consumption of a limited amount of electrolyte and the corresponding irreversible capacity loss. In addition, the cathodic decomposition products typically increase the interfacial resistance, which accelerates the electrical isolation of the fine particles. (iii) Electrolyte penetration and thinning of the base layer. The porous surface layer allows the electrolyte to approach the unreacted Al matrix preserved in the base layer. The fresh Al matrix has relatively low resistance to electronic and ionic conductivity, and thus the Li ions would prefer to react with the base layer rather than the high resistance surface layer. If the base layer is completely lithiated to brittle LiAl phase, the Al foil would be readily pulverized, leading to a rapid depletion of the capacity.

Based on these phenomena, preventing the excessive formation of a porous structure and maintaining a stable interface between the Al-foil anodes and the electrolyte would be a primary task to improve structural stability and cyclability. Focusing on the Al foil side, adjusting the composition and microstructure would be a potential strategy to control the morphological change during cycling. However, although various Al alloy systems have been established in the field of structural materials, the design guidelines for their use as anode materials in lithium batteries are still at a rudimentary stage. Recently, researchers have reported the effects of various alloy additions (*e.g.*, Si and In) in Al-foil anodes with liquid- or solid-state electrolytes.[11,12] For example, Al-1%Si foil has been found to exhibit superior cyclability compared to high purity Al foils in liquid electrolytes.[11] However, the reaction mechanism of Si addition during cycling is not yet clearly understood.

Therefore, to reveal the roles of alloy additions in Al-foil anodes and establish the design guidelines, in this work, we prepared a series of Al-Si foils with Si addition in the range of 0–4 wt% (weight percentage) and investigated how the Si distribution affects the mechanical and electrochemical properties of the Al matrix in electrode reactions. The Al-Si alloy typically has high strength and good workability in foil rolling, which is a suitable choice for studying the effects of alloy additions in Al-foil anodes. The X-ray diffraction (XRD) pattern and the scanning electron microscopy (SEM) observation of the Al-*x*Si foils (x = 0, 0.6, 1, 2, 4 wt%) showed that Si was uniformly distributed in the Al matrix as a solid solution when the concentration was less than 1%. Further increasing the Si concentration to over 1% facilitated the agglomeration of large Si particles randomly localized in the Al matrix and reduced the amount of uniformly distributed Si in the Al matrix. The cycle tests of the $LiCoO_2$‖Al-*x*Si full cells indicated that the cyclability is positively correlated with the amount of uniformly distributed Si in the Al matrix, and Al-1%Si showed superior performance in the concentration range of 0–4%. The SEM observation of the Al-*x*Si foils cycling up to 30 cycles indicated that the formation of a porous structure in the surface layer was significantly suppressed in Al-1%Si. Besides, high purity 99.99%Al and Al-4%Si showed a similar morphology change during cycling, indicating that the agglomerated large Si particles have minor effects on the electrode performance. Based on the calculated electromotive force (emf) and the phase diagram, the uniformly distributed Si in the Al matrix would form amorphous Li–Si(-Al) regions, pining the Al matrix during delithiation, preventing intergranular cracking and excessive formation of porous structures. On the other hand, the presence of the Li–Si(-Al) regions in the Al matrix and the relatively stable interface between the foil anode and the electrolyte tend to limit the lithium extraction, causing a large capacity loss in initial cycles, which requires further improvement to facilitate the interdiffusion of Li and Al inside the matrix.

Results and discussion

Characteristics of Al-*x*Si foils

Fig. 1a shows the phase diagram of the Al-Si binary system,[13] which is a typical eutectic system without intermetallic compounds. For the fcc-Al phase, Si has a solid solubility up to about 2 wt% at eutectic temperature (575 °C). This solid solubility range decreases as the temperature decreases and is almost zero below 300 °C. Thus, from a thermodynamic viewpoint, the Si addition to the Al-*x*Si foils would form a diamond-type Si phase at room temperature. To confirm the phase formation, XRD profiles of the Al-*x*Si foils (x = 0, 0.6, 1, 2, 4 wt%) were obtained and are compared in Fig. 1b. Interestingly, the XRD peaks of the Si phase were not observed in Al-0.6%Si and were clearly observed in Al-1%Si and those of higher Si concentrations. This suggests that a certain amount of Si addition could be dissolved in fcc-Al to form a solid solution phase, referred to as Al(Si), due to kinetic effects. Fig. 1c shows the SEM images and EDX mapping of Al and Si on the foil surface. For 99.99%Al ("4NAl") and Al-0.6%Si, both Al and Si show essentially uniform distribution. It should be noted that the signal of Si detected on the 4NAl foil was caused by the integration of background noise without an obvious Si peak in the EDX spectra (see Fig. S1†). The uniform distribution of Si in the Al-0.6%*x*Si foil confirmed that the Si addition was basically present in the Al(Si) phase without precipitation. In contrast, for Al-1%Si and those with higher Si concentration, Si was agglomerated to large particles, where the voids of Al were observed in the EDX mapping. These Si particles would

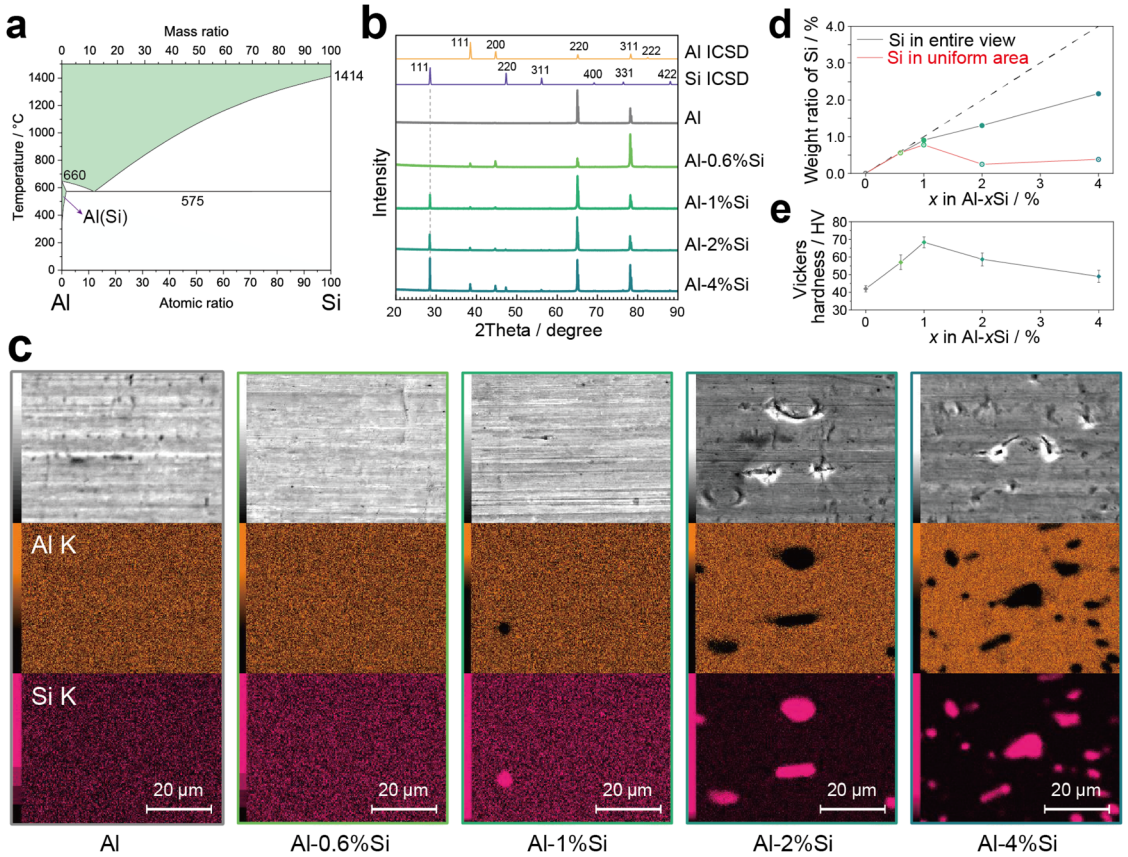

Fig. 1 Properties of different Al-*x*Si foils ($x = 0$, 0.6, 1, 2, 4 wt%). (a) Phase diagram of the Al-Si binary system. At room temperature, the Al-Si alloy would separate to fcc-Al and diamond-Si phases without compounds. (b) XRD patterns of the Al-*x*Si foils. The Si peaks were not observed in Al-0.6%Si, suggesting that the Si addition was present in the fcc-Al phase as a solid solution. (c) SEM images (upper row) and element mapping of Al (middle row) and Si (lower row) by EDX on different Al-*x*Si foils. Note that the Si detected in the high purity Al foil was caused by integrating the background noise without an identifiable peak (Fig. S1†). (d) Weight ratios of Si in the uniform distribution areas and the entire view based on the EDX mapping shown in (c). The amount of Si dissolved in the Al matrix was significantly decreased as agglomerated Si particles increased. (e) Vickers hardness of the Al-*x*Si foils. Al-1%Si shows the highest hardness, resulting from solid solution strengthening caused by the high Si concentration in the Al phase.

correspond to the XRD peaks of the Si phase, as shown in Fig. 1b. In addition, the Si concentration in the Al(Si) phase changed significantly with the appearance of agglomerated particles. Fig. 1d shows the Si concentration calculated in different areas based on the EDX mapping in Fig. 1c. The Si concentration in the entire view (gray solid line with markers) increased in proportion to the prepared compositions (dashed line). For Al-2%Si and Al-4%Si, the EDX composition was obviously lower than the prepared composition, which would be because localization of Si particles inside the foils caused underestimation from the shallow surface. Among the Al-*x*Si foils, the Si concentration in the uniform area (red solid lines with markers), *i.e.*, the Al(Si) phase, reached its maximum in the Al-1%Si foil and then decreased in Al-2%Si and Al-4%Si. In the low concentration range ($x < 1\%$), the long average distance between the Si atoms would kinetically hinder the nucleation and crystal growth of the Si phase during casting of the alloy ingots. As a result, the Si atoms can be uniformly distributed in the Al matrix as a solid solution. As the Si concentration increases ($x \geq 1\%$), the Si atoms readily agglomerate with each other to form the Si phase during casting, leading to the significant increase of the Si particles and the decrease of the uniformly distributed Si in the Al(Si) phase. Since the Si distribution markedly affects the microstructure, the Vickers hardness values of the Al-*x*Si foils were measured to estimate the change in mechanical properties and are compared in Fig. 1e. The highest Vickers hardness was observed in the Al-1%Si foil. The changes in hardness showed a relationship with the amount of uniformly distributed Si (red line in Fig. 1d), where the high Si concentration in Al(Si) would enhance the solid solution strengthening and increase the hardness.

Electrode properties of Al-*x*Si foil anodes

Cycle tests of the Al-*x*Si foil anodes were conducted in full cells with a $LiCoO_2$ cathode. The charge process was in a constant current–constant voltage mode (CCCV) and the discharge process was in a constant current mode (CC). The operating voltage range was set to 4.2–3.4 V, which is comparable to that of commercial lithium-ion batteries. Specifically, the cells were first charged to 4.2 V at a current density of 0.6 mA cm^{-2} (1/5 C

for $LiCoO_2$) and then the voltage was held at 4.2 V until the current density reduced to 0.06 mA cm^{-2} (1/50 C). After a 10 min rest, the cells were subsequently discharged at 0.6 mA cm^{-2} until the cell voltage reached 3.4 V. The maximum capacity in each process was set to 3 mA h cm^{-2}, which was the specification capacity of the commercial $LiCoO_2$ cathode sheet. It should be noted that because the electromotive force (emf) of the lithiation reaction of the Al-foil anodes is about 0.4 V *vs.* Li^+/Li,[12] the cut-off voltages of the present $LiCoO_2$||Al-*x*Si cells correspond to a potential range of 4.6–3.8 V *vs.* Li^+/Li for the $LiCoO_2$ cathode. Therefore, the Li^+ extraction from the $LiCoO_2$ cathode can exceed the specification threshold ($Li_{0.5}CoO_2$, about 4.3 V *vs.* Li^+/Li). The excess capacity supply would accelerate the degradation of the $LiCoO_2$ cathode, but can compensate for the capacity loss and improve the cyclability of the Al-*x*Si anodes. For the Al-*x*Si foil anodes, the areal capacity of 3 mA h cm^{-2} corresponds to the theoretical capacity of about 11 μm-thick Al to form LiAl. Since the Al-*x*Si foils were 50 μm thick, the ratio of the surface layer (active materials) in the Al-*x*Si foils was about 22%. Thus, the specific capacity of the whole Al-*x*Si foils would be about 220 mA h g^{-1}. This value is higher than the capacity of a graphite anode with the same areal capacity (3 mA h cm^{-2}) assembled with a 10 μm-thick Cu current collector.[5] Besides, since Si can alloy with Li up to $Li_{21}Si_5$ (4008 mA h g^{-1} for Si), the theoretical capacity increases with increasing the Si concentration, *i.e.* about +10% for Al-4%Si compared to 4NAl, see Table S1.†

Fig. 2a shows the capacity retention of the full cells with different Al-*x*Si foil anodes (x = 0, 1, 4 wt%). Among the foils, 4NAl showed a rapid degradation within 30 cycles. In contrast, the Al-1%Si anode showed significantly improved cyclability to about 120 cycles. The Al-4%Si anode improved the capacity retention in the first 20 cycles compared to Al-1%Si, but subsequently degraded in 60 cycles. Fig. 2b shows the accumulative capacity loss calculated by summing the differences in charge and discharge capacities in each cycle. Among the Al-*x*Si

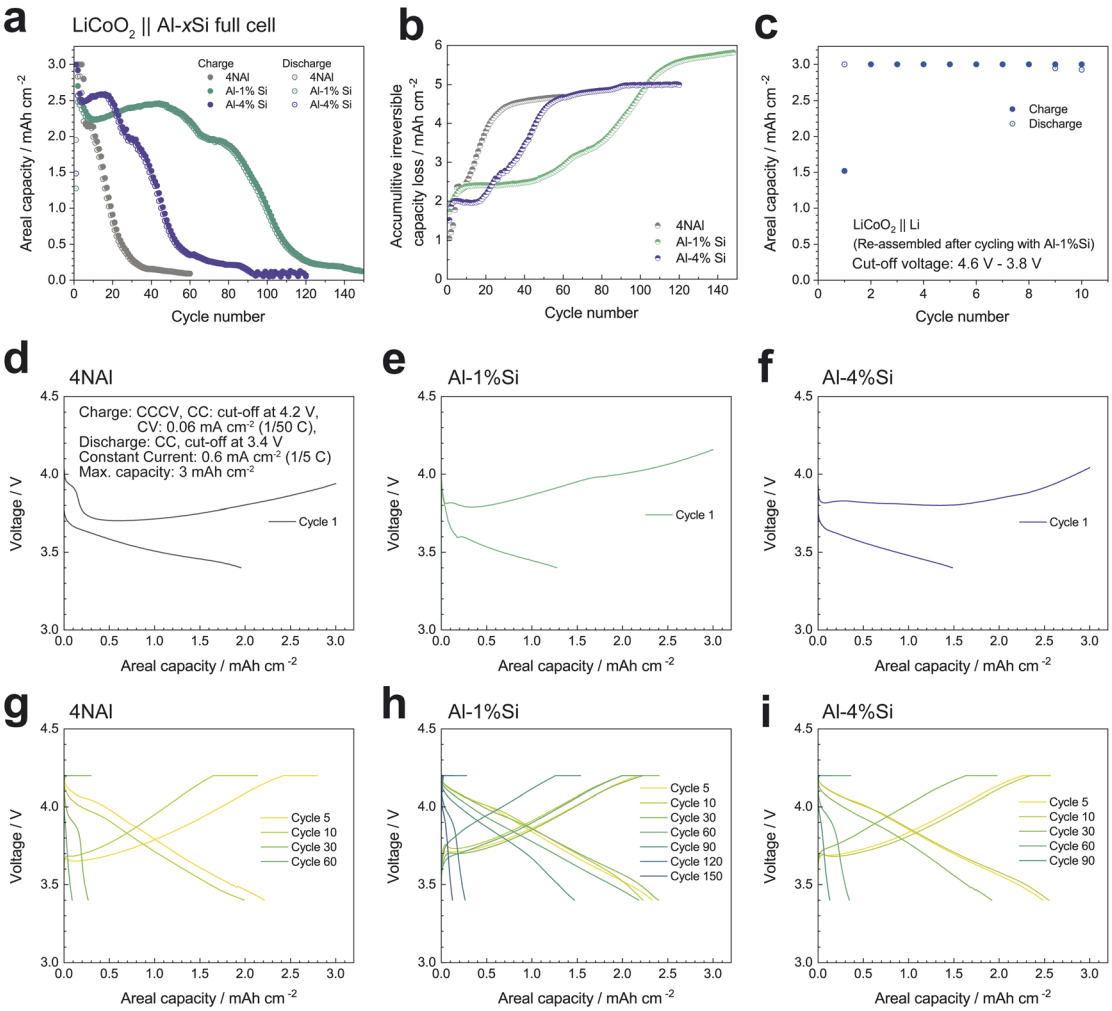

Fig. 2 Cycle tests of Al-*x*Si foil anodes using 2032-type coin cells with $LiCoO_2$ cathodes. (a) Capacity retention during cycling of different Al-*x*Si anodes. (b) Accumulative capacity loss during cycling calculated by summing the capacity differences between each charge and discharge process. (c) Reversible capacity of the $LiCoO_2$ cathode after cycling with Al-1%Si. The $LiCoO_2$ cathode was re-assembled into a half cell with a Li metal foil counter electrode. Voltage profiles in the first cycle of (d) the 4NAl, (e) the Al-1%Si and (f) the Al-4%Si anodes. Voltage profiles of several representative cycles during cycling of (g) the 4NAl, (h) the Al-1%Si and (i) the Al-4%Si anodes.

foils, the Al-1%Si anode showed a remarkably slow increase in the irreversible capacity compared to those of 4NAl and Al-4%Si. As shown in Fig. 2c and S2,† the $LiCoO_2$ cathodes after cycling basically maintained layered structures and retained certain reversible capacity in re-assembled half cells with a Li metal counter electrode. Therefore, the capacity degradation of the $LiCoO_2$||Al-*x*Si cells can be mainly attributed to the irreversible reactions that occurred on the Al-*x*Si anodes. Typically, the irreversible reactions consist of the following processes: (i) diffusional Li atom trapping in the LiAl and Al phases;[8] (ii) electrical isolation of LiAl particles and porosification during delithiation; (iii) electrolyte decomposition on the freshly exposed Al surface. Li trapping occurs most significantly in the first cycle and gradually proceeds in the subsequent cycles. Fig. 2d–f show the voltage profiles in cycle 1 of the cells with 4NAl, Al-1%Si, and Al-4%Si anodes, respectively. The Al-1%Si anode showed a low coulombic efficiency of about 43%, compared to 66% for 4NAl and 50% for Al-4%Si. The coulombic efficiency is correlated with the amount of the uniformly distributed Si and the corresponding hardness of the Al-*x*Si foils (Fig. 1e). The hard matrix phase retards the reaction kinetics, increasing the overpotential and decreasing the coulombic efficiency. The Li atoms kinetically trapped in the surface layer can be confirmed by the Li mapping as shown in Fig. S3.† Since the capacity loss due to the diffusional Li trapping is basically a one-time chemical process, the irreversible capacity loss is moderated in the subsequent cycles. Besides, because the formation of a porous structure during Li extraction would shorten the Li diffusion distance to the surface, the trapped Li would be gradually released during cycling. In contrast, capacity loss due to the isolation of LiAl particles and the electrolyte decomposition is basically irreversible reactions. Fig. 2g–i show the voltage profiles of several representative cycles of the Al-*x*Si foils in cycle tests. The cell voltages during charging rose rapidly to a cut-off voltage of 4.2 V as the cycle number increased, indicating that the mobile Li^+ ions in the $LiCoO_2$ cathode were depleted during cycling. As also shown in Fig. 2b, the Al-1%Si anode has slow capacity degradation especially between cycles 10 and 60, which is distinguished from the other cases. Since the capacity loss due to the isolation of LiAl particles and the electrolyte decomposition would be strongly related to the formation of an interface between the foil anode and the electrolyte, the morphological changes of the Al-*x*Si foil anode due to the addition of Si have a significant contribution to its cyclability.

Morphological changes during repeated (de)lithiation

To investigate the structural changes during cycling, we conducted cycle tests of the Al-*x*Si foils in half cells with Li counter electrodes. The lithiation process was conducted to a fixed areal capacity of 2 mA h cm^{-2} in each cycle and the delithiation process was conducted until the cell voltage reached 1 V. The capacity change is shown in Fig. S4.† The Al-*x*Si electrodes were disassembled from the half cells after 1, 3, 10, 15, and 30 cycles ended in a delithiated state. Fig. 3a–c compare SEM images of the surface and the cross-section views of 4NAl, Al-1%Si, and Al-4%Si, respectively. For 4NAl, a crevasse-like Al matrix was observed in the initial cycles and gradually changed to uniformly fine particles (Fig. 3a). The porosification of the Al matrix would be attributed to the self-organization during delithiation, which progressively decreases the particle size of the recrystallized Al phase. In addition, the surface layer became thicker, and the base layer became thinner during cycling. This indicates that the fine Al particles in the surface layer did not have sufficient chemical activity, while the remaining fresh Al matrix in the base layer was progressively lithiated as active materials. The loss of chemical activity of the fine Al particles in the surface layer can be attributed to the inefficient electrical connection between the particles and the high interfacial resistance caused by the electrolyte decomposition products. Compared to 4NAl, Al-1%Si showed a distinctively different morphology change during cycling, where the crevasse-like structure was maintained without significant porosification within the 30 cycles (Fig. 3b). The limited increase in the surface area can also be confirmed by nitrogen absorption measurements (Fig. S5†). For Al-4%Si, the morphological change was close to the case of 4NAl, although the amount of Si addition was even higher than that of Al-1%Si (Fig. 3c). Considering the Si distribution as shown in Fig. 1, it suggests that the uniformly distributed Si in the Al(Si) phase (solid solution) would play a significant role in suppressing the excessive formation of porous structures and in improving the electrode performance, compared to the agglomerated Si particles precipitated in the Al matrix. Similar effects were also observed at different current densities (Fig. S6†). For the influence of the agglomerated Si particles, since the formation of Li–Si alloys would cause a huge volume expansion (Si to $Li_{4.4}Si$, +400%), the agglomerated Si particles in the Al matrix would accelerate the cracking of the surface layer during lithiation, negating the benefits and resulting in rapid pulverization as observed in Al-4%Si.

To quantify the structural degradation of the Al-*x*Si anodes, the thickness of the surface and base layers was measured from the cross-section views. Fig. 3d compares the thickness of the surface layer of the different Al-*x*Si foils during cycling. The ideal thickness is 7.5 μm for an areal capacity of 2 mA h cm^{-2}. For 4NAl, the thickness of the surface layer linearly increased as the cycle number increased. At cycle 30, the thickness of the surface layer was over 10 times thicker than the initial value. In contrast, the thickness of the surface layers of Al-1%Si and Al-4%Si showed a rapid increase in the initial 10 cycles and subsequently stayed constant in several cycles. After that, the thickness of the surface layer began to increase again, which was slower for Al-1%Si compared to Al-4%Si. The change of the thickness of the surface layer showed a strong correlation with the capacity change in cycle tests (Fig. 2a and S3†), indicating that a more stable structure results in higher cyclability.

On the other hand, as shown in Fig. 3e, the thickness of the base layer showed an opposite trend to that of the surface layer. Since the initial thickness of the Al-*x*Si foils is 50 μm, the preserved unreacted base layer would be 50–7.5 = 42.5 μm thick. This expected thickness of the base layer was obtained in cycle 1, but it gradually decreased as the cycles were repeated. The consumption rate of the base layer slightly varied

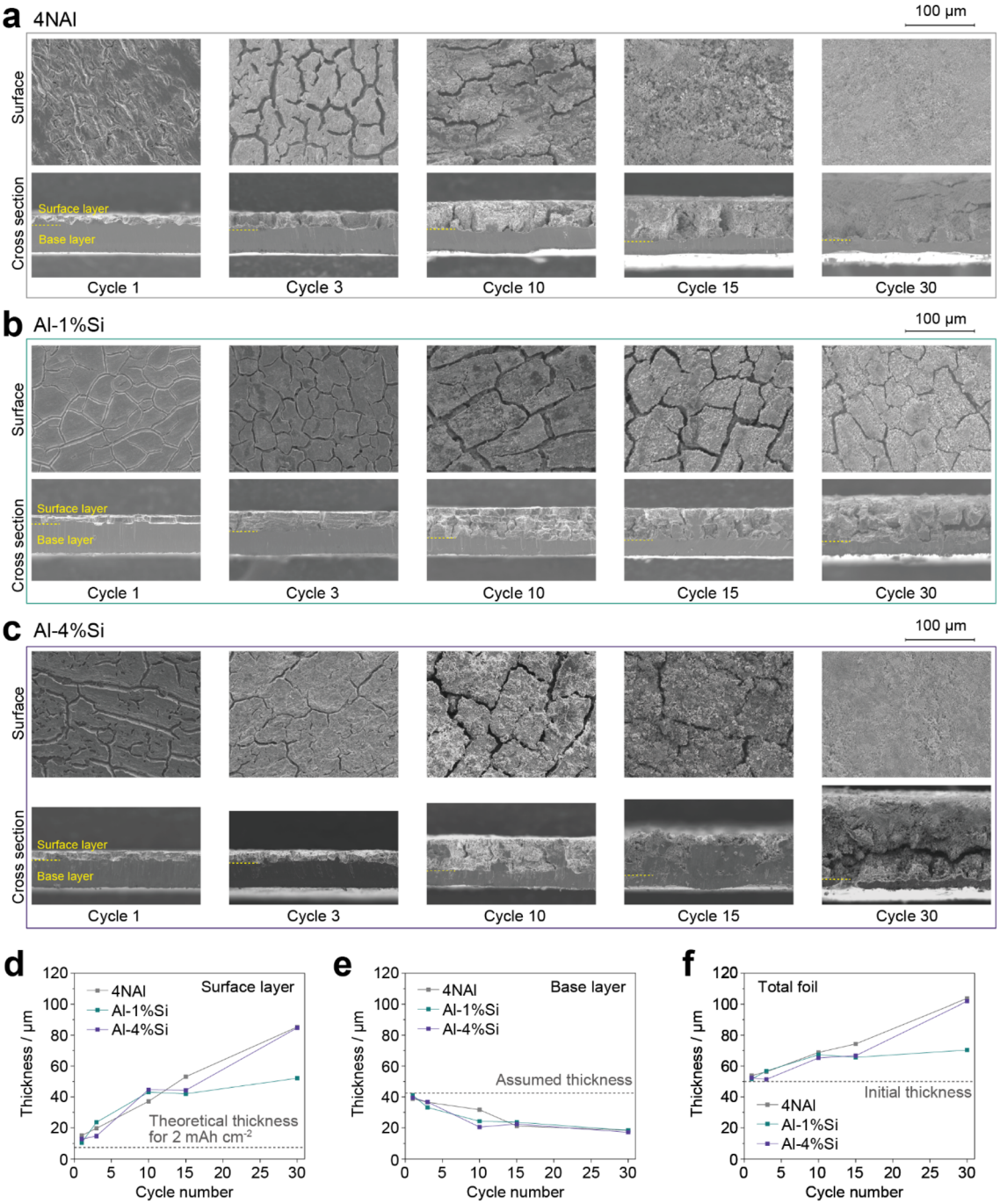

Fig. 3 Morphological changes of (a) 4NAl, (b) Al-1%Si and (c) Al-4%Si foil anodes during cycling in half cells with Li counter electrodes. Al-1%Si shows limited formation of porous structures during cycling. (d–f) Change in the thickness of the Al-*x*Si foils during cycling. (d) The surface layer. (e) The base layer. (f) The whole Al-*x*Si foil. The surface layer is reacted with Li as the active material, and the base layer remains as the unreacted Al matrix in the Al-*x*Si foil anodes.

depending on the amount of Si addition up to cycle 15, but by cycle 30, the thickness of the base layer was almost the same for all Al-*x*Si foils. Since the Al matrix is basically homogeneous throughout each Al-*x*Si foil independent of the Si concentration, it is difficult to confine the inserted Li in the surface layer and prevent it from penetrating the base layer. As a result, the base layer is gradually consumed during cycling regardless of the uniform distribution or agglomeration of the Si addition. As a possible strategy, inserting a lithiation potential gap between the surface layer and base layer by preparing clad Al foils can effectively prevent the Li penetration into the base layer.[10] Fig. 3f shows the thickness change of the whole Al-*x*Si anodes. Al-1%Si showed a distinctive small thickness change in the cycles 10–30, which corresponds to its better cyclability.

Role of the Si addition in the Al(Si) phase

Based on the electrochemical measurements and morphological observations, it is found that the uniformly distributed Si atoms in the Al matrix as a solid solution, *i.e.*, Al(Si), have a major influence on the electrode reaction rather than the agglomerated large Si particles. To further understand the role of the Si addition, we compared the morphological changes of 4NAl and Al-1%Si in the first lithiation and delithiation processes in detail. Fig. 4a–b show the voltage profiles and the cross sections of the 4NAl and Al-1%Si electrodes, respectively. The (de)lithiation was conducted in a half cell with a Li metal counter electrode. The lithiation proceeded up to 3 mA h cm^{-2} and then the delithiation proceeded up to a cut-off voltage of 1 V. The current density was 0.5 mA cm^{-2}. The Al-*x*Si anodes before and after the (de)lithiation were cut using Ar ion milling and then the cross sections were observed with a backscattered electron detector (BED) attached to a SEM. In the BED images, the LiAl phase is relatively dark compared to the Al phase, which can be used to distinguish the different phases. The agglomerated Si particles showed a light color in the BED images compared to the Al and LiAl phases. For 4NAl, the initial lithiation formed a dark 18 μm-thick LiAl layer from a 9 μm-thick Al layer, which confirmed that the +100% volume expansion occurred only in the out-of-plane direction of the Al foil. After 1 mA h cm^{-2} was delithiated, interestingly, areas of the recrystallized Al phase were formed in several regions penetrating the LiAl layer, indicating that the Li atoms were not uniformly extracted from the surface. Besides, several cracks were observed in the delithiated areas, allowing the electrolyte to penetrate the surface layer and facilitate the delithiation. When the delithiation proceeded to the cut-off voltage, there were many fine cracks in the surface layer and a small amount of LiAl (dark area) remaining in the 4NAl anode. This was consistent with the low irreversible capacity in the voltage

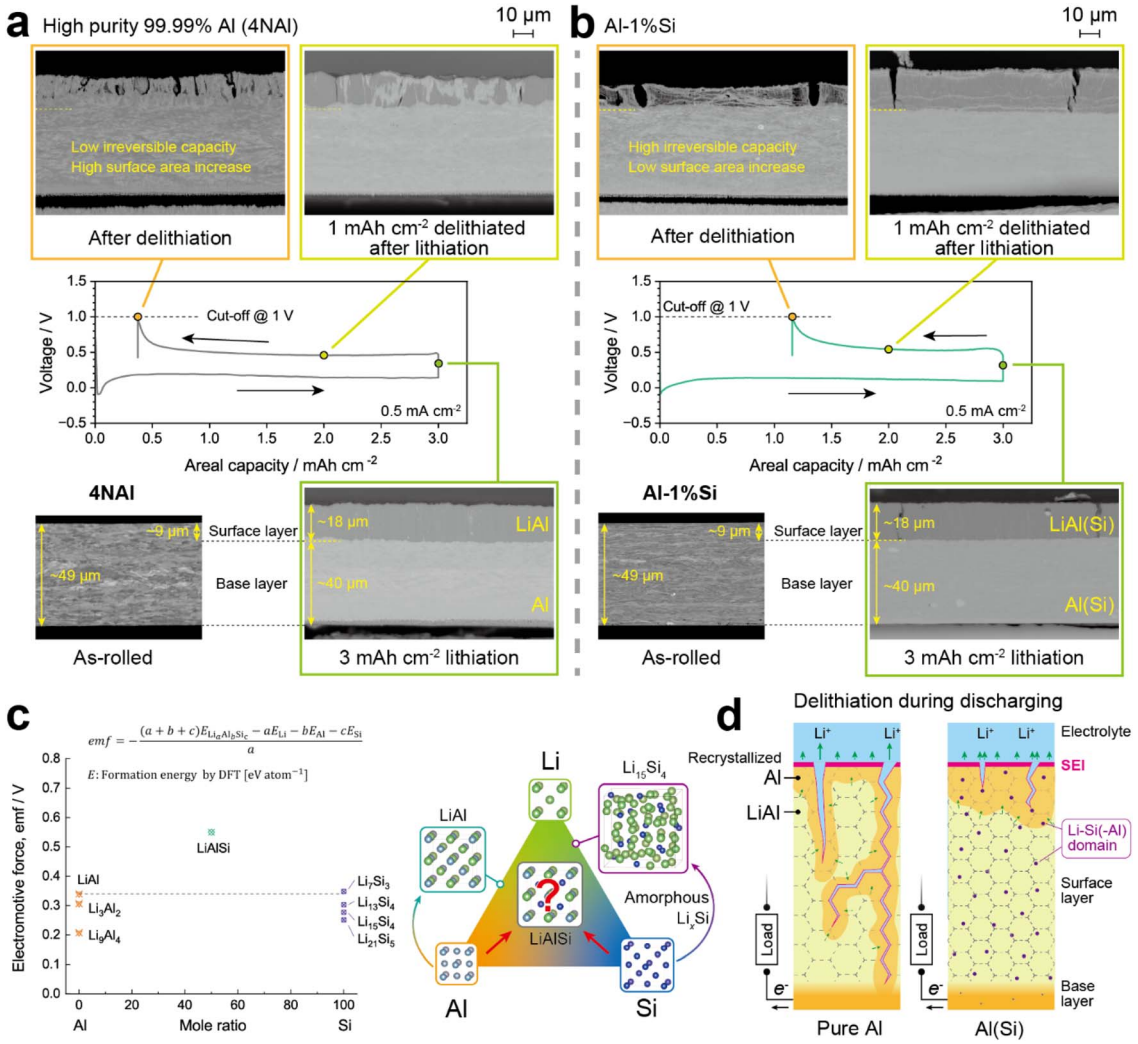

Fig. 4 Role of Si addition in Al-*x*Si foil anodes. (a and b) Morphological changes during the initial lithiation and delithiation process on (a) 4NAl and (b) Al-1%Si foils. (c) Calculated electromotive force (emf) of the lithiation phases in the Li–Al-Si ternary system. The formation energies used in the calculation were computed based on density functional theory (DFT) and taken from the Materials Project. The right side illustrates the possible phase transition pathway based on the phase diagram. (d) Schematic figure of the effects of the uniformly distributed Si in the Al matrix on the formation of the porous structure in the self-organization during delithiation.

profile. However, the increase of the surface area due to the cracks would cause progressive electrolyte decomposition and porosification of Al matrix, as shown in Fig. 3a.

On the other hand, for Al-1%Si, the lithiation process showed a similar behavior to that for 4NAl. The higher hardness (smaller particle size) of Al-1%Si may also be inherited to the LiAl phase, helping to maintain the uniform lithiation and the one-directional volume expansion. Several vertical cracks were observed after lithiation, which may be caused by grain boundary failure due to the isotropic volume expansion of the agglomerated large Si particles during lithiation. After 1 mA h cm^{-2} delithiation, the recrystallized Al phase formed mainly on the foil surface and in some layered regions inside the LiAl layer. Compared to 4NAl, there were few cracks formed during delithiation, which contributes to a more uniform delithiation behavior. When the delithiation reached the cut-off voltage, the crevasse-like surface layer shrinked without obviously increasing cracks. In this situation, the Li would be preferentially extracted from the regions of low stress constraints, such as the surface and some grain boundaries. Since the Al matrix has a very low solid solubility of Li compared to the LiAl phase, surrounded by the Al matrix would be difficult to delithiate and cause diffusional Li trapping.[8] These phenomena consequently lead to a large irreversible capacity in the initial cycles, while the limited increase in the surface area suppresses the progressive electrolyte decomposition and the porosification of the Al-1%Si foil anode during cycling.

From these results, it can be concluded that uniformly distributed Si atoms in the Al(Si) phase have a pinning effect on the recrystallized Al and LiAl particles during delithiation, preventing cracks from entering the grains and also propagating along the grain boundaries. Fig. 4c shows the electromotive force of the lithiation reaction of the typical alloy phases in the ternary system. The formation energy (E) values were based on density functional theory (DFT) and were taken from the Materials Project (see Table S2†). The ternary compound LiAlSi has an electromotive force of 0.55 V in the lithiation reaction, which is the highest value among the stable phases. Below it, the emfs of the series of Li–Si binary compounds have similar or lower values than the LiAl phase. From the calculated emfs, during lithiation, the Si additions in the Al matrix would first tend to form a ternary LiAlSi phase and then separate into the mixture of Li–Si and Li–Al binary compounds. However, because the Si-related phases were not experimentally detected as a crystal phase by XRD after lithiation (Fig. S7†), the Si atoms in the Al matrix would form amorphous Li–Si(-Al) domains, as have been reported on the Si anodes for lithium-ion batteries.[14] As shown in the schematic illustration in Fig. 4d, when the Li atoms are extracted and the remaining Al phase is recrystallized, the Li–Si(-Al) domains would be retained due to the higher emf and sluggish kinetics and restrict the volume contraction of the surrounding Al matrix in the self-organization. Therefore, the grain boundary failure (cracks) that occurs on the surface would be impeded at the shallow surface without growing into the matrix. To prove this reaction mechanism, further characterization techniques are yet required to provide more direct evidence for the phase transformation of the alloy additions in the Al matrix.

Conclusions

In this work, the effects of Si addition to Al-xSi foil anodes on electrode properties and morphological changes were investigated in a concentration range of 0–4%. The Si added to the Al matrix is distributed in two main forms: for additions lower than 1%, there was no detectable Si phase, and the Si atoms were uniformly dispersed in the Al matrix as a solid solution; for additions higher than 1%, the Si atoms agglomerate into large particles and a diamond-type Si phase was observed. The cycle tests of the Al-xSi anodes with $LiCoO_2$ cathodes showed that the capacity retention is positively correlated with the number of uniformly dispersed Si atoms in the Al matrix, where Al-1%Si showed much longer cyclability compared to high purity 4NAl and Al-4%Si. Morphological observations of cross sections during cycling showed that, for Al-1%Si, the Al matrix phase maintained a crevasse-like structure and the excessive porosification of recrystallized Al particles during delithiation was significantly suppressed. Combined with the calculated emfs of the compounds in the Li–Al-Si ternary system, the formation of amorphous Li–Si(-Al) from the uniformly distributed Si atoms in the Al matrix was suggested to play a key role in preventing the cracks growing into the Al matrix, consequently improving the structural and chemical stability and the cyclability. However, the limited surface increase also retards the Li diffusion kinetics, which causes a high irreversible capacity loss in the initial cycles. Besides, since the cracks are not completely avoided, the electrolyte penetration to the base layer still causes the consumption of the preserved fresh Al matrix in the base layer. To overcome these shortages, further improvement of Al-foil anodes in liquid electrolytes requires adjustment of alloy additions to facilitate Li diffusion while preventing cracking and the subsequent electrolyte penetration. As a potential strategy, we consider that controlling the alloy addition (M) to adjust the mixing enthalpy or interaction parameters between the elements in the Al–Li–M ternary system would be possible to enhance both the stability and the kinetics of Li extraction. For example, the use of alloy additions that do not form alloy phases with Li can have a distinct effect on the diffusion kinetics of Li in the Al matrix compared to the Si case. In addition to material design, the optimization of the other battery components (*e.g.* electrolyte,[15–17] see Fig. S8†) is also essential to maximum the cycle performance of Al-foil anodes towards practical applications.

Experimental

Materials preparation

High purity (99.99%) Al foil (4NAl) and Al-xSi foils (x = 0.6, 1, 2, 4 wt%) were produced by Sumitomo Chemical Co., Ltd. For the preparation of the Al-xSi foils, corresponding amounts of high purity (99.999%) Si chips were added into molten Al and then cast into ingots and rolled into foils. The foil thickness was standardized to 50 μm.

Materials characterization

The crystal structure of the different Al-*x*Si foils was evaluated by X-ray powder diffraction (XRD) using a diffractometer (SmartLab, Rigaku Co.) with Cu Kα radiation. The morphology of the Al-*x*Si foils was observed with a field emission scanning electron microscope (FE-SEM, JSM-7200F, JEOL Ltd). The Al and Si mapping was conducted using an energy dispersive X-ray (EDX) spectrometer attached to the FE-SEM. The hardness of each Al foil was measured with a micro-HV tester (HMV-G21DT, Shimadzu Corporation). A test force of HV0.05 (490.3 mN) was employed and held for 15 s. More than six points were measured for each sample with appropriate intervals.

Electrochemical experiments

2032-type coin cells (Hohsen Corp.) and three-electrode coin cells (SB7, EC-FRONTIER Co., Ltd) were employed to conduct electrochemical experiments. For $LiCoO_2$||Al-*x*Si full cells, 2032-type coin cells were assembled with a $LiCoO_2$ cathode (Hohsen Corp). The $LiCoO_2$ cathode had a specification capacity of 3 mA h cm^{-2}. For Al-*x*Si||Li half cells, three-electrode coin cells were assembled with Li foils (Honjo Metal Co. Ltd) as the counter electrode (CE) and reference electrode (RE). For the electrolytes, 1 M $LiPF_6$ in EC : DMC (50 : 50 vol%) was purchased from Merck KGaA. A 25μm-thick polyethylene (PE) separator (W-SCOPE CORPORATION) was soaked with the electrolyte and used to separate the electrodes in the coin cells. The electrolyte volume in the 2032-type cell was 50 μL and in the three-electrode coin cell was 200 μL. The coin cells were assembled in an argon-filled glovebox. The electrochemical measurements were controlled using a potentiostat (VMP-3 or VSP-300, Bio-Logic SAS). After electrochemical tests, the Al-*x*Si foils were washed with tetrahydrofuran (99.5%, FUJIFILM Wako Pure Chemical Corporation) and subsequently dried in an argon atmosphere to remove the electrolyte before further measurements.

Data availability

The data supporting this article have been included as part of the ESI.†

Author contributions

T. I. and T. Y. conceived the study. H. L. designed the research plan. S. N. and H. L. conducted the main part of the experiments. S. M., Y. N., H. H. and T. K. prepared the Al-*x*Si foils. W. L. conducted some supplementary measures. N. L. O conducted the nitrogen absorption measurement. H. L. summarized the results and wrote the manuscript.

Conflicts of interest

S. M., Y. N., H. H., T. K. and T. Y. are employees of Sumitomo Chemical Co., Ltd. The other authors declare no conflicts of interest.

Acknowledgements

This work is a joint research project contracted between Tohoku University and Sumitomo Chemical Co., Ltd. This work is partly supported by the Grant-in-Aid for Scientific Research (S) number 23H05452 commissioned by the Japan Society for the Promotion of Science (JSPS).

References

1 B. M. L. Rao, R. W. Francis and H. A. Christopher, *J. Electrochem. Soc.*, 1977, **124**, 1490.
2 J. O. Besenhard, J. Yang and M. Winter, *J. Power Sources*, 1997, **68**, 87–90.
3 X.-X. Chen, H. Huang, L.-Y. Yi, Z.-H. Wang, Z.-C. Song, J.-X. Xing, C.-H. Wei, A.-J. Zhou and J.-Z. Li, *Rare Met.*, 2024, **44**, 121–134.
4 T. Ichitsubo, S. Yagi, T. Doi, S. Yukitani, K. Hirai and E. Matsubara, *J. Electrochem. Soc.*, 2011, **159**, A14–A17.
5 H. Li, T. Yamaguchi, S. Matsumoto, H. Hoshikawa, T. Kumagai, N. L. Okamoto and T. Ichitsubo, *Nat. Commun.*, 2020, **11**, 1584.
6 T. Wada, T. Ichitsubo, K. Yubuta, H. Segawa, H. Yoshida and H. Kato, *Nano Lett.*, 2014, **14**, 4505–4510.
7 T. Chen, A. C. Thenuwara, W. Yao, S. E. Sandoval, C. Wang, D. H. Kang, D. Majumdar, R. Gopalaswamy and M. T. McDowell, *Batteries Supercaps*, 2023, **6**, e202200363.
8 P. J. Crowley, K. P. Scanlan and A. Manthiram, *J. Power Sources*, 2022, **546**, 231973.
9 C. Wang, T. Chen, Y. Liu, D. H. Kang, D. Majumdar, R. Gopalaswamy and M. T. McDowell, *ACS Energy Lett.*, 2023, **8**, 2252–2258.
10 H. Li, S. Nishimura, Y. Nakata, S. Matsumoto, T. Yamaguchi, H. Hoshikawa, T. Kumagai and T. Ichitsubo, *J. Mater. Chem. A*, 2023, **11**, 23311–23318.
11 S. S. Sharma, P. J. Crowley and A. Manthiram, *ACS Sustain. Chem. Eng.*, 2021, **9**, 14515–14524.
12 Y. Liu, C. Wang, S. G. Yoon, S. Y. Han, J. A. Lewis, D. Prakash, E. J. Klein, T. Chen, D. H. Kang, D. Majumdar, R. Gopalaswamy and M. T. McDowell, *Nat. Commun.*, 2023, **14**, 3975.
13 A. L. Udovsky, V. N. Karpushkin and E. A. Kozodaeva, *Calphad*, 1995, **19**, 245–277.
14 P. Limthongkul, Y.-I. Jang, N. J. Dudney and Y.-M. Chiang, *Acta Mater.*, 2003, **51**, 1103–1113.
15 R. Tan, J. Zhang, K. Liu, X. Zhu, R. Gao, Q. Zhang, Y. Wang, X. Ai and J. Qian, *Adv. Funct. Mater.*, 2024, **34**, 2316341.
16 H. Li, M. Murayama and T. Ichitsubo, *Cell Rep. Phys. Sci.*, 2022, **3**, 100907.
17 H. Li, D. Shimizu, R. Jin, T. Zhang, D. Horikawa, K. Nagaya, H. Tsubouchi, H. Yamaguchi, M. Okumura and T. Ichitsubo, *J. Mater. Chem. A*, DOI: 10.1039/d4ta07531e.